24th COBEM - 2017

24th ABCM International Congress of Mechanical Engineering
December 3-8, 2017, Curitiba, PR, Brazil

COBEM-2017-1607
NUMERICAL STUDY OF THE JSM HIGH-LIFT CONFIGURATION USING A RANS APPROACH

Ricardo Galdino da Silva
Instituto de Aeronáutica e Espaço, DCTA/IAE/ALA, São José dos Campos, SP, 12228-904, Brazil
ri_galdino@yahoo.com.br

Leonardo Motta Maia de O. Carvalho
Instituto Tecnológico de Aeronáutica, DCTA/ITA, São José dos Campos, SP, 12228-900, Brazil
leonardo.mmoliva@gmail.com

João Luiz F. Azevedo
Edson Basso
Instituto de Aeronáutica e Espaço, DCTA/IAE/ALA, São José dos Campos, SP, 12228-904, Brazil
joaoluiz.azevedo@gmail.com ; edsonbss@gmail.com

Abstract. *The goal of present effort is to compare our in-house numerical code results with the ones available for complex high-lift configurations (Wing and Body - WB and Wing, Body, Pylon, and Nacelle - WBPN) developed by JAXA. Due to the high complexity of high-lift configurations, this comparison will be very useful since our in-house CFD code is, right now, passing through the process of verification numerical methodology and enhancement of the turbulence models available. Our code, called BRU3D by our research group, solves Reynolds-averaged Navier-Stokes equations using the finite-volume method on unstructured grids. The aerodynamics coefficients obtained for results of WB configuration is in good agreement with experimental results for most angles of attacks. The stall for this configuration occurs earlier than shown by experimental results, in addition, the shear-stress lines pattern reveals a different stall trigger, when it is compared with the oil flow pattern. The results obtained for WBPN configuration present not only a good agreement with experimental for aerodynamics coefficients but, also, for shear-stress lines patterns. The stall characteristics are correctly predicted for this configuration.*

Keywords: *RANS, High-Lift Devices, CFD, Unstructured Mesh, Complex Geometries*

1. INTRODUCTION

In modern transonic commercial aircraft, the speed differences between cruise, landing, and take-off are very high. Usually, a mid-sized commercial aircraft cruises at transonic Mach numbers very close to unity. In contrast to these high cruise Mach numbers, landing and takeoff commonly reach much lower values, varying between 0.1 to 0.25. These low speeds imply that, without any modifications in its geometry, wings designed to perform well in transonic Mach numbers could not generate high lift coefficients at low speeds. High-lift devices (slats and flaps) are meant to solve this problem, once its main purpose is to increase the lift coefficient by increasing the stall angle of attack (slats) and increasing the lift generated at zero angle of attack (flaps).

High-lift devices are very relevant to the industry, this, as a consequence, makes the complex physics involving high-lift devices important as well. Thus, a deep understanding of all physics futures presents on such a flow is relevant, when the final issue is optimizing the maximum lift coefficient for landing configuration or lift over drag for a takeoff configuration. The confluence of the boundary layer with wakes, shock-waves interacting with boundary layers, separation due to adverse pressure gradient and complex vortex structures (horseshoe vortex) are, for instance, some flows futures present in a typical simulation of high-lift configurations. These flow futures, which are inherent to such a complexity geometries, makes the prediction of high-lift devices aerodynamic coefficient by means of numerical tools, a challenge even for the most sophisticated CFD software available today.

Our intention when comparing this type of configuration during our code checks is exactly that. To benchmark our numerical tool and know-how for high-lift condition calculations over complex geometries. In this context, the goal behind the present work is to compare results available in the literature with the ones obtained with our code. called by our research group as BRU3D, our in-house CFD code is currently under development at the aerodynamic division

inside DCTA/IAE. This code solves the Reynolds-averaged Navier-Stokes (RANS) equations using finite volume method applied to unstructured grids. Since turbulence plays an important role in predicting the flow behaviour over high-lift as in most of the engineering application, the Spalart-Allmaras turbulence model, which was proposed by Spalart and Allmaras (1992) and Spalart and Allmaras (1994), is used in a compressible RANS formulation. It is important, as well, to mention that the meshes for this type of configuration are easily close to 100 million cells. To deal with meshes this size, the code uses FORTRAN 90 programming language allied with dynamic memory allocation and Message Passing Interface parallel paradigm.

In the next sections, the numerical methodology used to solve RANS equations will be briefly explained, the compressible formulation of Spalart-Allmaras turbulence model will be also exposed. On the section 4the numerical results for high-lift Jaxa Standart Model (JSM) will be compared with experimental results obtained from the 3rd AIAA CFD High Lift Prediction Workshop (HiLiftPW-3) website. Finally, to close this effort some concluding remarks will be addressed by the authors.

2. THEORETICAL AND NUMERICAL FORMULATION

The RANS equations are, in a mathematical context, very complex beasts to deal with. Being a system of non-linear partial differential equations, a numerical methodology have to be used in order to extract a valid solution field from then. The BRU3D code does it using implicit time-stepping for numerical robustness in time, Roe's (Roe, 1981) flux-difference splitting for spatial resolution. The turbulence model used is Spalart-Allmaras turbulence model to evaluate the eddy-viscosity. In the next sub-sections, the Reynolds-averaged Navier-Stokes equations, the Spalart-Allmaras turbulence model, and the numerical methodologies will be briefly explained.

2.1 Reynolds-Averaged Navier-Stokes Equations

The flows considered in the present effort are described by the 3-D compressible Reynolds averaged Navier-Stokes (RANS) equations and it is assumed to be fully turbulent. It is worth to mention that averaged process for compressible flow is called Favre averaged. The Navier-Stokes equations, in its dimensions form, after Favre's averaged process are given by:

$$\frac{\partial Q}{\partial t} + \nabla \cdot (E_e - E_\nu) = 0 \tag{1}$$

in which Q is given by

$$Q = [\rho \ \rho u \ \rho v \ \rho w \ \ e]^T \tag{2}$$

where ρ is the density, u, v, w are the vector velocity (**v**) components and e is the total energy per unit volume, which is difined as:

$$e = \rho \left[e_i + \frac{1}{2} \left(u^2 + v^2 + w^2 \right) \right] \tag{3}$$

and the inviscid (E_e) and viscous (E_ν) flux vectors are given by

$$E_e = \begin{Bmatrix} \rho \mathbf{v} \\ \rho u \mathbf{v} + p\widehat{i}_x \\ \rho v \mathbf{v} + p\widehat{i}_y \\ \rho w \mathbf{v} + p\widehat{i}_z \\ (e+p)\mathbf{v} \end{Bmatrix} \qquad E_\nu = \begin{Bmatrix} 0 \\ \left(\tau^l_{xj} + \tau^t_{xj}\right)\widehat{i}_j \\ \left(\tau^l_{yj} + \tau^t_{yj}\right)\widehat{i}_j \\ \left(\tau^l_{zj} + \tau^t_{zj}\right)\widehat{i}_j \\ \beta_j \widehat{i}_j \end{Bmatrix} \tag{4}$$

The shear-stress tensor is defined as:

$$\tau^l_{ij} = \mu_l \left(\frac{\partial u_i}{\partial x_j} + \frac{\partial u_j}{\partial x_i} - \frac{2}{3} \frac{\partial u_m}{\partial x_m} \delta_{ij} \right) \tag{5}$$

in which u_i is velocity component, and x_i is referent to coordinate the system. The dynamic viscosity μ_l is determined by Sutherland law. The static pressure is given by the perfect gas law, which can be write as:

$$p = (\gamma - 1)\left[e - \frac{1}{2}\left(u^2 + v^2 + w^2\right)\right] \tag{6}$$

The work done by viscous force and the heat transfer, β_j, is difined as $\beta_j = \left(\tau^l_{ji} + \tau^t_{ji}\right) u_i - q_j$. Moreover, the heat transfer is computed by:

$$q_j = -\gamma\left(\frac{\mu_l}{Pr} + \frac{\mu_t}{Pr_t}\right)\frac{\partial(e_i)}{\partial x_j}. \tag{7}$$

The unknown Reynolds stress tensor, τ^t , is modeled within BRU3D via linear (Boussinesq hypothesis) and non-linear edge viscosity models. In the present effort, only the linear eddy viscosity is used, on which the Reynolds stress tensor is given by:

$$\tau^t_{ij} = \mu_t\left[\left(\frac{\partial u_i}{\partial x_j} + \frac{\partial u_j}{\partial x_i}\right) - \frac{2}{3}\frac{\partial u_m}{\partial x_m}\delta_{ij}\right] - \frac{2}{3}\rho k\delta_{ij} \tag{8}$$

in which the k is the turbulent kinetic energy and μ_t is the eddy viscosity. In our case, the term related to k will be incorporated by the pressure, once the turbulence model selected does not have an explicit relation for k. The turbulence model selected is Spallart-Allmaras turbulence model proposed by Spalart and Allmaras (1992) and Spalart and Allmaras (1994). The transport equation used for this model is presented in Sec. 2.2

The RANS equations (Eq. 1) and the turbulence model equations according to finite volume method are given by

$$V_i\frac{\partial Q_i}{\partial t} = -\sum_{k=1}^{nf}\left(E_{e_k} - E_{\nu_k}\right)\cdot S_k = -RHS \tag{9}$$

in which the subscript k stands for properties computed in the k^{th} face, and nf represents the number of faces, which form the i^{th} control volume. To obtain Eq. 9, it is assumed constant fluxes through volumes faces and also constant Q_i proprieties inside the volume faces. The first assumption is a sufficient approximation to obtaining $2nd$ order accuracy in the currently available flux computation schemes. In the convective flux computation, a Roe flux-difference splitting scheme (Roe, 1981) is assumed. To achieve $2nd$ order accuracy in space, primitive properties are linearly reconstructed at cell faces with MUSCL algorithm (van Leer, 1979) in conjugation with limiter function, such as Venkatakrishnan minmod, van Albada or super bee limiters that are currently available in BRU3D. The present effort uses Venkatakrishnan (Venkatakrishnan, 1993) as limiter function. In addition, the diffusion term is discretized using a method that computes nonoscillatory derivatives at the cell faces.

A $1st$ order backward Euler implicit non-linear scheme for Eq. 9 is given by

$$V_i\frac{\Delta Q^n_i}{\Delta t} = -RHS\left(Q^{n+1}_i\right) \tag{10}$$

here, $\Delta Q^n_i = Q^{n+1}_i - Q^n_i$. The linearisation use an expansion of $RHS\left(Q^{n+1}_i\right)$ about ΔQ^n_i as in

$$RHS\left(Q^{n+1}_i\right) = RHS\left(Q^n_i\right) + \frac{\partial RHS\left(Q^n_i\right)}{\partial Q^n_i}\Delta Q^n_i + O\left(\Delta Q^n_i\right)^2 \tag{11}$$

and leads to the 1^st order accurate implicit scheme:

$$V_i\frac{\Delta Q^n_i}{\Delta t} + \frac{\partial RHS\left(Q^n_i\right)}{\partial Q^n_i}\Delta Q^n_i = -RHS\left(Q^n_i\right) \tag{12}$$

More detail in how calculate the residue $\left(RHS\left(Q^n_i\right)\right)$, the Jacobian $\left[\frac{\partial RHS(Q^n_i)}{\partial Q^n_i}\right]$, and flux can be found in Bigarella and Azevedo (2009).

2.2 Turbulence Closure: Spalart-Allmaras Model

The turbulence model used in the present effort is the Spalart-Allmaras model (Spalart and Allmaras, 1994). It is a one equation model for a modified kinematic eddy viscosity $\tilde{\nu}$. Moreover, this is widely used by the aerospace community. The transport equation used in SA model, in its compressible version, is given by:

$$\frac{\partial(\rho\tilde{\nu})}{\partial t} + \frac{\partial(\rho u_j\tilde{\nu})}{\partial x_j} = \rho c_{b1}\hat{S}\tilde{\nu} - \rho c_{w1} f_w \left(\frac{\tilde{\nu}}{d}\right)^2 + \\ + \frac{1}{\sigma}\left[\frac{\partial}{\partial x_j}\left(\rho\left(\nu+\tilde{\nu}\right)\frac{\partial\tilde{\nu}}{\partial x_j}\right) + \rho c_{b2}\frac{\partial\tilde{\nu}}{\partial x_i}\frac{\partial\tilde{\nu}}{\partial x_i}\right] - \frac{1}{\sigma}\left(\nu+\tilde{\nu}\right)\frac{\partial\rho}{\partial x_i}\frac{\partial\tilde{\nu}}{\partial x_i} \tag{13}$$

The first and second trip terms are left out from Eq. 13. The turbulent eddy viscosity is obtened from :

$$\mu_t = \rho\tilde{\nu} f_{v1} \tag{14}$$

in which $f_{v1} = \frac{\chi^3}{\chi^3+c_{v1}^3}$, $\chi = \frac{\tilde{\nu}}{\nu}$.

In order to avoid $\tilde{S}$ to become negative, a limiting method is used, which is given by:

$$\hat{S} = \begin{cases} \Omega + \overline{S} & \text{if } \overline{S} \geq -c_2\Omega \\ \Omega + \frac{\Omega(c_2^2\Omega + c_3\overline{S})}{(c_3-2c_2)\Omega - \overline{S}} & \text{if } \overline{S} < -c_2\Omega \end{cases} \tag{15}$$

$$\overline{S} = \frac{\hat{\nu}}{\kappa^2 d^2} f_{v2} \tag{16}$$

in which d is the distance from cell center to nearest wall and $\kappa = 0.41$ is the von KÃąrmÃąn constant. The term $\Omega = \sqrt{2W_{ij}W_{ij}}$ is the magnitude of the antisymmetric part of the velocity gradiente tensor. Moreover, the antisymmetric tensor is computed from $W_{ij} = \frac{1}{2}\left(\frac{\partial u_i}{\partial x_j} - \frac{\partial u_j}{\partial x_i}\right)$.

The rest of the variables and functions found in Eq. 13 are given by:

$$f_{v2} = 1 - \frac{\chi}{1+\chi f_{v1}} \tag{17}$$

$$f_w = g\left[\frac{1+c_{w3}^6}{g^6+c_{w3}^6}\right]^{1/6} \tag{18}$$

$$g = r + c_{w2}(r^6 - r) \tag{19}$$

$$r = \min\left[\frac{\tilde{\nu}}{\tilde{S}\kappa^2 d^2}, 10\right] \tag{20}$$

The constants are $c_{b1} = 0.1355$, $c_{b2} = 0.622$, $\sigma = \frac{2}{3}$, $c_{w2} = 0.30$, $c_{w3} = 2$, $c_{v1} = 7.1$, $c_2 = 0.7$ and $c_3 = 0.9$. This new equation is solved fully coupled with the Navier-Stokes equation. The production, destruction and cross-diffusion terms present in Eq. 13 are treated implicitly. Thus, the Jacobian for these terms is also calculated.

3. THE JSM MODEL

The geometry that is under study right now is the JSM (Jaxa high-lift Configuration Standard Model) Yokokawa *et al.* (2010). This wind-tunnel model represents a mid-sized airliner jet conceptualized from scratch by JAXA. The preliminary design constrains were established as follows. The maximum take-off weight of 100,000 lbs, cruising and maximum Mach numbers of 0.8 and 0.84 respectively, cruising range of 2300 nm, the landing distance of 4000 ft and take-off distance of 5000 ft.

The half-span wind-tunnel model seen in Fig. 1 represents the configuration developed by JAXA, in its complete assembly, it has a circular fuselage, flap track fairings (FTF), pylon, nacelle and high-lift devices. The general dimensions of the model include 2.3 m of half-span and 4.9 m of fuselage length. Other important dimensions of the model are described in Table 1. The JSM (Jaxa Standart Model) is the high-lift system that will be studied in a nominal landing configuration with support brackets on, and nacelle/pylon on/off. The experiment used a semi-span model with a 60 mm peniche standoff, but the computations are “free air”, without the wall and the semi-span effect.

Table 1. Important dimensions of the JSM model.

Important Dimensions of the JSM model	
Half span lengh	2.3m
Mean aerodynamic chord	0.5292m
Wing area (half span)	1.233m^2
Sweep angle	33 degrees
Aspect ratio	9.42
Taper ratio	0.333

Figure 1. JAXA model in it’s full configuration Yokokawa *et al.* (2010).

The lift coefficient, drag coefficient and pitching moment at Re equal to 1.93 million (Mean aerodynamic chord) and Mach number equal to 0.172 at 3rd AIAA CFD High Lift Prediction Workshop (HiLiftPW-3) website, since the JSM configurations were used at HiLiftPW-3. It is also available pressure coefficient data for several sections along the wing spam of JSM model. However, this data is not used in the present effort. In addition, oil visualization was performed and as also made available. This type of visualization is very useful to identify separations over the wing, which is directed related to stall characteristics of aircraft configuration. This type of visualization can be directly compared with numerical shear stress lines at the model surface. The available data is related to a configuration with pylon nacelle on and off.

All meshes for WB configuration and WBPN configuration are hybrids meshes, which means that they are composed of prismatic cells in the near wall region, in order to have a better representation of the boundary layer, and combinations of pyramidal cells and tetrahedral cells in the rest of computational domain. In addition, it also has a mesh refinement at the wing wake region. These meshes have been obtained from HiLiftPW-3 website and the name given to these meshes was E-JSM_UnstrMixed_ANSA. Moreover, these meshes were classified with a medium refinement level, the WB configuration mesh has 109 million cells and the WBPN has 120 million cells.

4. RESULTS

In this section, the numerical results obtained with the BRU3D code will show and compare with experimental data available for high lift WB configuration and WBPN configuration at Mach number equal to 0.172 and Re number equal to 1.93 million. The experimental results that will be presented are based on data with an without corrections. The corrections try to eliminate wind tunnel walls effects and semi-spam effects.

The lift curve, drag polar and also the pitching moment are shown in Fig. 2 for JSM WB configuration. It is possible to observe from Fig. 2(a) a good agreement between numerical and experimental results of lift coefficient from angles of attack to 10.47 deg. However, for angles of attack granter than 10.47 deg, the lift coefficient is underestimated.Moreover, the stall occurs earlier in numerical results. It occurs 18.58 deg for numerical results and around 20 deg. for experimental results. On Fig. 2(b), in which the drag polar is present, it possible to observe a difference between numerical results and experimental results. The pitching moment (Fig. 2(c)) present a good agreement with experimental results for angles of attack up to 10.47 deg, for angles greater than that the results present an increasing discrepancy.

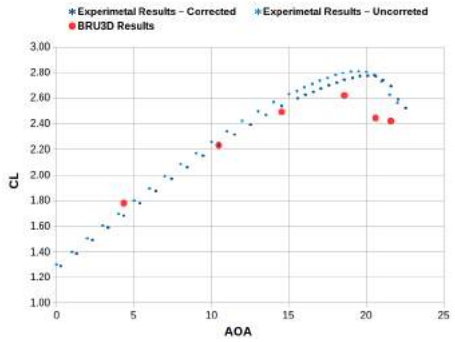

(a) Lift Curve

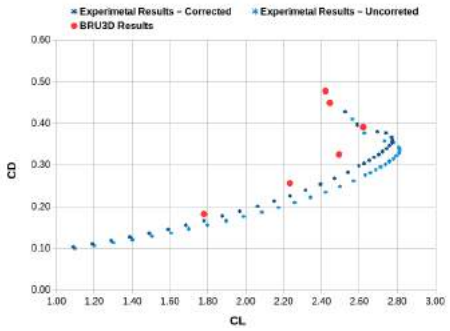

(b) Drag Polar

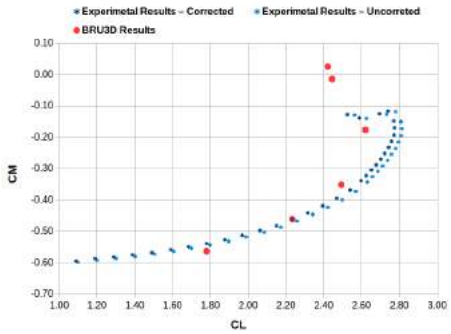

(c) Pitching Moment

Figure 2. Aerodynamics coefficients for JSM WB configuration.

The Figs. 3 and 4 show the comparison of oil flow visualization and shear-stress lines of JSM WB configuration for angle of attack 18.58 deg and 21.57 deg, respectively. The first angle is placed before stall and the shear-stress lines present patterns(Fig. 3(b)) similar to oil flow patterns (Fig. 3(a)). It is possible to identify on Fig. 3(a) and Fig. 3(a) the presence of horseshoe vortex in the wing body junction, the flow separation at the wing tip and also the effects of slats brackets. The second angle (21.57 deg) is placed after the stall and the experiential and numerical shear-stress lines are not similar. The horseshoe effects seem to be more strong on the experimental, at the outboard region of the wing numerical results present a separation that has not been observed on experimental visualization. In addition, the pattern at the wing tip observed in experimental and numerical results are similar. The Experimental results present a stall triggered by the horseshoe vortex at the wing root. On the other hand, the numerical results stall starts further outboard along the wingspan, which seems to be triggered by slats brackets.

The lift curve, drag polar and also the pitching moment are shown in Fig. 5 for JSM WBPN configuration. The lift coefficient obtained from numerical results have a good concordance with experimental results for angles of attack used on simulation, the only exception is the biggest angle of attack. All these observations came from Fig. 5(a). The tendency of drag polar is captured by simulation results (5(b)), however, the magnitude discrepancy needs to be improved. The pitching moment has a similar behavior of experimental results for angle smaller than 18.58 deg, see 5(c).

The Fig. 6 and Fig. 7 show the comparison of oil flow visualization and shear-stress lines of JSM WBPN configuration for angle of attack equal to 18.58 deg and 21.57 deg, respectively. For the first angle of attack (18.58 deg 6), the shear-

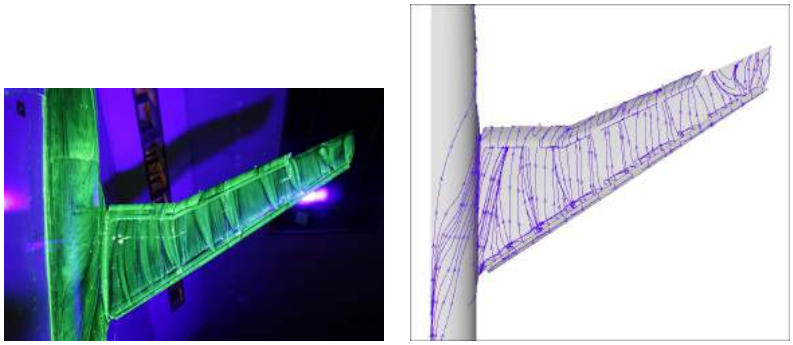

(a) Experimental - Oil flow visualization (b) Numerical - Shear-stress lines

Figure 3. Comparison between oil flow visualization and shear-stress lines. JSM WB @ AOA = 18.58 deg

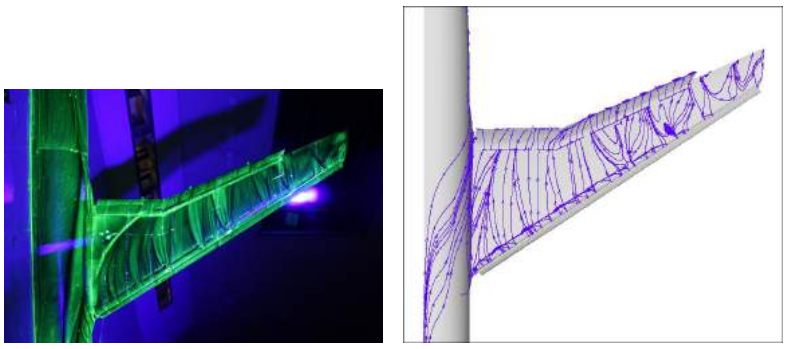

(a) Experimental - Oil flow visualization (b) Numerical - shear-stress lines

Figure 4. Comparison between oil flow visualization and shear-stress lines. JSM WB @ AOA = 21.57 deg

stress lines have a pattern almost identical to the pattern observed on the oil flow visualization. On those visualization techniques, it is possible to identify horseshoe vortex, nacelle wake from its inboard and outboard part affecting the flow under the wing, and the wing tip separation, all those flow futures is present in both experimental and numerical visualization. The effect of horseshoes on the numerical results seems to be stronger than on the experimental results. On the other hand, the nacelle wake effects for numerical results seems to be weaker when it is compared to experimental. Wing tip separation size for experimental results is smaller than for numerical results. Those comparisons are made to look into the size of regions on main element affected by each flow feature. For second angle of attack (21.57 deg - Fig. 7), it is possible to identify not only for experimental experimental results, but also for numerical The horseshoe vortex at the wing body junction region, nacelle wake effects on the main element, the effects of the slats support and the wing tip separation. From the oil flow visualization and shear-stress lines, it's possible to infer that the horseshoe vortex effect is stronger on the experimental results. Moreover, the wing tip separation size for numerical results is bigger than the experimental one.

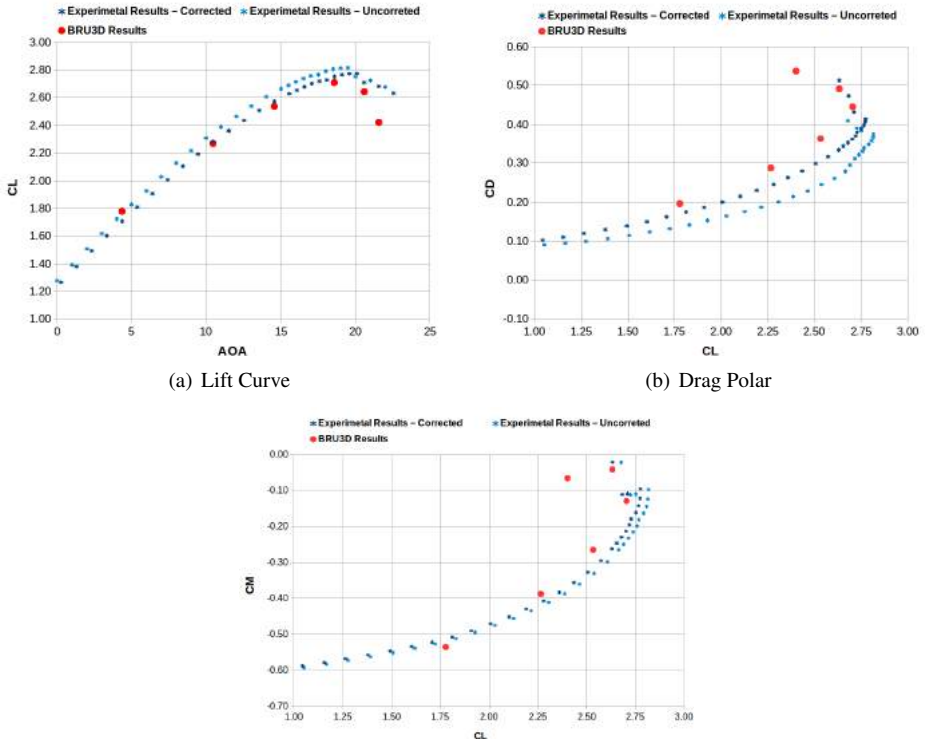

(a) Lift Curve (b) Drag Polar

(c) Pitching Moment

Figure 5. Aerodynamics coefficients for JSM WB configuration.

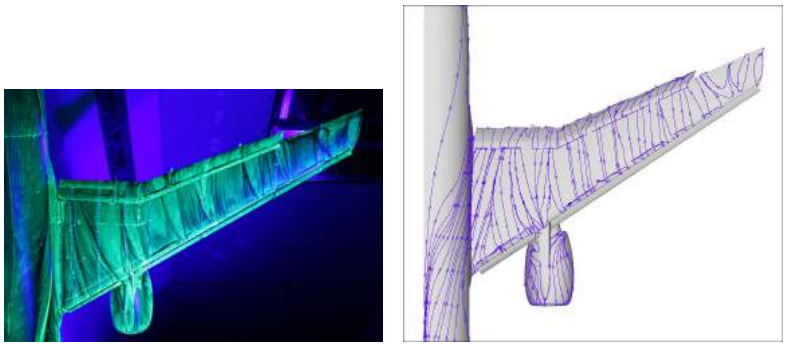

(a) Experimental - Oil flow visualization (b) Numerical - Shear-stress lines

Figure 6. Comparison between oil flow visualization and shear-stress lines. JSM WBPN @ AOA = 18.58 deg

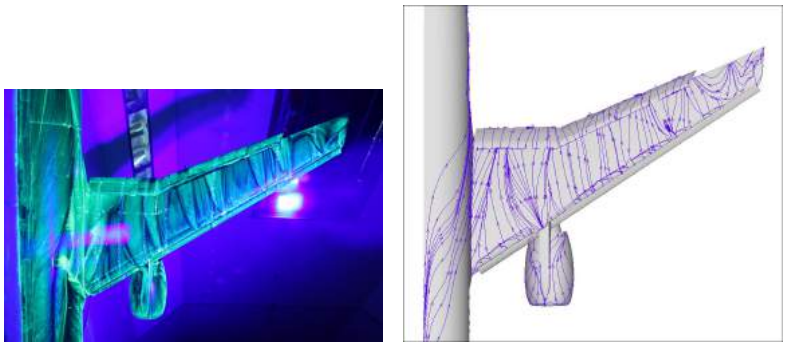

(a) Experimental Oil flow visualization (b) Numerical - Shear-stress lines

Figure 7. Comparison between oil flow visualization and shear-stress lines. JSM WBPN @ AOA = 21.57 deg

5. CONCLUDING REMARKS

For both JSM configuration, WB and WBPN, the comparison between experimental results and numerical results for aerodynamics coefficients show a good agreement whit experimental results when the flow is attached. The exception is the drag coefficient for WB configurations which the highest discrepancies of all coefficients. The experimental results of JSM WB configuration show that the stall is triggered by the horseshoe vortex at the wing root. However, the numerical results show the stall starts further outboard along the wing span. For JSM WBPN configuration both, numerical and experimental results, show similar stall characteristics. The experimental results and the numerical results show stall as consequence of wing root horseshoe vortex and nacelle-wake separation on inboard wing panel. These flow features prevent the growth of the wing load at the inboard wing panel region.

6. ACKNOWLEDGMENTS

The authors gratefully acknowledge the partial support for this research provided by Conselho Nacional de Desenvolvimento Científico e Tecnológico, CNPq, under the Research Grants No. 309985/2013-7, No. 400844/2014-1 and No. 443839/2014-0. The authors are also indebted to the partial financial support received from Fundação de Amparo à Pesquisa do Estado de São Paulo, FAPESP, under the Research Grant No. 2013/07375-0.

7. REFERENCES

Bigarella, E.D.V. and Azevedo, J.L.F., 2009. "A unified implicit cfd approach for turbulent-flow aerospace-configuration simulations". In AIAA Paper No. 2009-1473*, 47th AIAA Aerospace Sciences Meeting Including The New Horizons Forum and Aerospace Exposition*. Orlando, FL.

Roe, P.L., 1981. "Approximatte riemann solvers, parameter vectors, and difference schemes". *Journal of Computational Physics*, Vol. 43, No. 2, pp. 357–372.

Spalart, P. and Allmaras, S., 1992. "A one-equation turbulence model for aerodynamic flows". In *30th Aerospace Sciences Meeting and Exhibit*. Reno, NV.

Spalart, P.R. and Allmaras, S.R., 1994. "A one-equation turbulence model for aerodynamic flows". *Recherche Aerospatiale*, Vol. 7, No. 1, pp. 5–21.

van Leer, B., 1979. "Towards the ultimate conservative difference scheme. v. a second-order sequel to godunov's method". *Journal of Computational Physics*, Vol. 32, No. 1, pp. 101–136.

Venkatakrishnan, V., 1993. "On the accuracy of limiters and convergence to steady state solution". In *Proceedings of the 31st Aerospace Sciences Meeting and Exhibit*. Reno, NV.

Yokokawa, Y., Murayamama, M., Uchida, H., k. Tanaka, Ito, T. and Yamamoto, K., 2010. "Aerodynamic influence of a half-span model installation for high-lift configuration experiment". In *48th AIAA Aerospace Sciences Meeting*.

8. RESPONSIBILITY NOTICE

The authors are the only responsible for the printed material included in this paper.